ARCHIVES OF ACOUSTICS
29, 1, 107–121 (2004)

THE RESPONSE OF HELMHOLTZ RESONATOR TO EXTERNAL EXCITATION. PART I: ACOUSTICALLY INDUCED RESONANCE

M. MEISSNER

Institute of Fundamental Technological Research
Polish Academy of Sciences
00–049 Warszawa, Świętokrzyska 21, Poland
e-mail: mmeissn@ippt.gov.pl

(*received 29 August 2003; accepted 15 December 2003*)

The first of two companion papers theoretical and experimental results are presented for a Helmholtz resonator subject to external excitation by an acoustic plane wave. The response of the resonator was analysed in terms of the relation between the pressure induced in the interior of the resonator and the driving pressure. Equations for the resonance frequency and the quality factor were developed for the cavity that was a rectangular parallelepiped with a centered circular orifice. The flow from the cavity had a constant velocity profile. The resonator was modelled by an equivalent impedance circuit, predicted from the classic theory of sound radiation, with an additional resistive term connected with the viscous action inside the orifice. The theoretical results were compared with experimental data for a frequency chosen so as to tune the system to the lowest resonance mode. The experiment has shown that the acoustic response of resonator was changed considerably when mechanical vibrations of the resonator elements were excited. A phenomenon of flow-induced resonance in the considered system geometry will be presented in the companion paper.

1. Introduction

The Helmholtz resonator has found application in a wide variety of technologically significant problems [1–3] and has been the subject of many papers [4–9]. Essentially, the resonator is a cavity of relatively large volume connected with the outside space through an orifice or neck. The classical physical model of the Helmholtz resonator includes an air spring (the cavity), a mass (the air mass in an orifice or neck plus co-vibrating mass) and a damper arising from the radiation of sound, and from the presence of viscosity forces. An extensive review of the lumped-elements approach (the spring-mass damper model) can be found in the work of INGARD [10]. The characteristic property of the resonator is its ability to absorb sound waves of a particular frequency, the so-called resonance frequency. Therefore in practical applications, it is important to determine the resonance frequency and absorption properties of the system as precisely

as possible since an inaccurate design can considerably reduce the efficiency of the device.

In the present paper the Helmholtz resonator in a form of rectangular parallelepiped with a circular orifice placed in an infinite rigid baffle is considered. The resonator is excited by a plane wave incident upon the baffle. The purpose of the theoretical part is to predict a response of the resonator to an acoustic excitation as a relation between the driving pressure and the pressure induced inside the resonator cavity. The result will be used to determine the resonance frequency, where the absolute value of a resonator impedance has a minimum, and the quality factor characterizing selective properties of the system. In the second part of the paper results of measurements of the resonator response for varying resonator length are presented. These results confirm the usefulness of the theoretical analysis. The experiment shows also that the resonator response may be considerably deformed when mechanical vibrations of the resonator elements are excited.

2. Theoretical model

The details of the resonator geometry are shown in Fig. 1. The excitation of the resonator is achieved by the plane pressure wave $p_i(z,t) = P_i e^{j(kz-\omega t)}$, where ω is the angular frequency, $k = \omega/c$ is the wave number and c is the sound speed. Since a driving acoustic signal consists of incident and reflected plane pressure waves, the amplitude P of the excitation is twice as large as P_i.

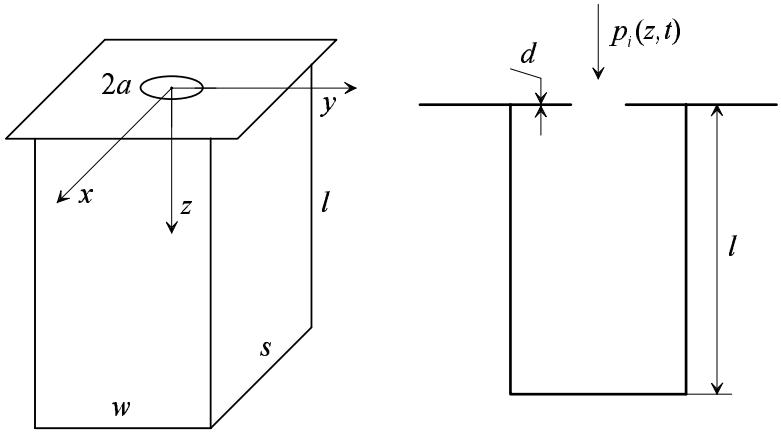

Fig. 1. Nomenclature and co-ordinate system for the resonator under consideration.

2.1. Pressure induced inside the cavity

The pressure p in the resonator interior can be determined with the aid of the classical theory of sound radiation, where the air flow through the orifice is modelled by an

oscillating piston [11]. If the origin of a cylindrical coordinate system (r, ϕ, z) lies at the center of the orifice and the plane $z = 0$ covers the baffle surface on the cavity side, then this theory yields the pressure p induced inside the cavity as (the factor $e^{-j\omega t}$ was excluded)

$$p(r,\phi,z) = -j\rho\omega u \int_0^{2\pi}\int_0^{a} G(r,\phi,z\,|\,r_s,\phi_s,z_s=0)\; r_s dr_s d\phi_s\,, \tag{1}$$

where ρ is the air density, u is the velocity amplitude in the resonator orifice, G is the Green's function in the resonator cavity and (r_s, ϕ_s, z_s) is the position of the source point. The function G is a solution of the wave equation and satisfies the boundary condition

$$\frac{\partial G}{\partial x}\left(x = \pm\frac{s}{2}\right) = \frac{\partial G}{\partial y}\left(y = \pm\frac{w}{2}\right) = \frac{\partial G}{\partial z}(z=0) = \frac{\partial G}{\partial z}(z=l) = 0\,, \tag{2}$$

then it may be expressed as follows [12]

$$G = j\sum_{m=0}^{\infty}\sum_{n=0}^{\infty} g_{mn} \begin{cases} \cos(k_{mn}z_s)[\sin(k_{mn}z) + \cos(k_{mn}z)\cot(k_{mn}l)], & z \geq z_s, \\ \cos(k_{mn}z)[\sin(k_{mn}z_s) + \cos(k_{mn}z_s)\cot(k_{mn}l)], & z \leq z_s. \end{cases} \tag{3}$$

The function g_{mn} in Eq. (3) is given by

$$g_{mn} = \frac{j\epsilon_{mn}}{A_c k_{mn}} \cos(2m\pi r\cos\phi/s)\cos(2m\pi r_s\cos\phi_s/s) \cdot \cos(2n\pi r\sin\phi/w)\cos(2n\pi r_s\sin\phi_s/w), \tag{4}$$

where $A_c = sw$ is the cross-sectional area of the cavity, $k_{mn} = \sqrt{k^2 - [(2m\pi/s)^2 + (2n\pi/w)^2]}$ and ϵ_{mn} is the Neumann factor, $\epsilon_{00} = 0$, $\epsilon_{m0} = \epsilon_{0n} = 2$, $\epsilon_{mn} = 4$ for $m, n > 0$. Using Eq. (1) together with Eqs. (3) and (4), the expression for the pressure p can be found as

$$p(r,\phi,z) = \frac{2j\rho ckU}{A_c}\sum_{m=0}^{\infty}\sum_{n=0}^{\infty} \frac{\epsilon_{mn}J_1(a\beta_{mn})\cos(2m\pi r\cos\phi/s)\cos(2n\pi r\sin\phi/w)}{a\beta_{mn}k_{mn}} \cdot[\sin(k_{mn}z) + \cos(k_{mn}z)\cot(k_{mn}l)], \tag{5}$$

where J_1 is the Bessel function of first order, $U = Au$ is the volume velocity in the orifice, A is the orifice area and $\beta_{mn} = \sqrt{(2m\pi/s)^2 + (2n\pi/w)^2)}$. The complex form of Eq. (5) results from a contribution of cross-modes to the resonator response.

2.2. Impedance of the resonator

The relation between the amplitude P of the driving pressure and the volume velocity U can be written as

$$P/U = Z = Z_e + Z_i + Z_o\,, \tag{6}$$

where Z_e and Z_i denote the exterior and interior impedances, respectively, and Z_o is the orifice impedance. For the circular orifice placed in an infinite baffle MORSE and INGARD [11] have made an exact calculation of the exterior impedance and found that

$$Z_e = \frac{\rho c}{A}\left[1 - \frac{J_1(2ka)}{ka} - \frac{jS_1(2ka)}{ka}\right], \tag{7}$$

where S_1 is the Struve function of first order. The real and imaginary components of Z_e represent respectively the loss resistance due to the radiation of acoustic energy into the surrounding medium and the reactance connected with the co-vibrating mass effect on the exterior side of the orifice. The interior impedance is defined as the ratio of the average pressure at the orifice to the velocity U. Using Eq. (5) one obtains

$$Z_i = \frac{\int_0^{2\pi}\int_0^a p(r,\phi,z=0)\; r dr d\phi}{AU} = \frac{4j\rho\omega}{A_c}\sum_{m=0}^{\infty}\sum_{n=0}^{\infty}\frac{\epsilon_{mn} J_1^2(a\beta_{mn})\cot(k_{mn}l)}{a^2 k_{mn}\beta_{mn}^2}, \tag{8}$$

where the zero order component in the series is the reactance for a plane wave motion inside the cavity. The thickness d of the orifice is assumed to be small, so the fluid inside the orifice acts as a mass and thus provides the orifice reactance. The additional component of Z_o, which was customarily included, is the viscous loss resistance [10], thus finally

$$Z_o = \frac{\sqrt{2\rho\mu\omega}}{A}\left(2 + \frac{d}{a}\right) - \frac{j\rho ckd}{A}, \tag{9}$$

where μ is the coefficient of viscosity, and the orifice reactance is negative because of the time dependence $e^{-j\omega t}$ of the incident wave.

2.3. Low-frequency approximation

In the following we will concentrate on the low-frequency range, where ω is much smaller than the lowest frequency of cross-modes. Since in this case the plane wave contribution is dominant, Eq. (5) for the pressure p assumes a simple form

$$p(z) = j\rho cU[\sin(kz) + \cos(kz)\cot(kl)]/A_c \tag{10}$$

and it is easy to see that a maximum of p appears at the bottom end of the cavity. This is the place, where a pressure in the resonator interior is usually measured, then owing to practical purposes a proper choice for z is to put $z = l$ in Eq. (10). In this case from Eq. (10) and Eqs. (6)−(9) one obtains the following expression

$$p(l) = \frac{j\rho cP}{A_c(R + jX)\sin(kl)}, \tag{11}$$

where $R = R_o + R_r$ is the resonator resistance and R_o is the real component of the orifice impedance Z_o and $R_r = \rho c k^2/2\pi$ is the radiation resistance in the low-frequency range. The reactance of the resonator is given by

$$X = \rho c \left[\frac{\cot(kl)}{A_c} - \frac{k(d+\Delta)}{A} \right], \tag{12}$$

where Δ is the sum of the external and internal end corrections

$$\Delta_e = \frac{8a}{3\pi}, \qquad \Delta_i = \frac{4\pi}{A_c} \sum_{m=0}^{\infty} \sum_{n=0}^{\infty} \frac{\chi_{mn} J_1^2(a\beta_{mn}) \coth(\beta_{mn} l)}{\beta_{mn}^3} \tag{13 a,b}$$

and $\chi_{00} = 0$, $\chi_{m0} = \chi_{0n} = 2$, $\chi_{mn} = 4$ for $m, n > 0$. Equation (13b) implies that due to the factor $\coth(\beta_{mn} l)$ the internal end correction Δ_i not only depends on the orifice and cavity transverse dimensions but also on the cavity length l. However, in most cases it is possible to assume $\coth(\beta_{mn} l) \simeq 1$ because this factor can considerably differ from unity for very shallow cavities only.

The internal end correction may be calculated by use of a numerical method. However, in some cases it is possible to find a simple expression for Δ_i. An important example for the practical use is a resonator with a square cross-section and a transverse dimension that does not exceed the cavity length. In this case from Eqs. (13a) and (13b) one obtains

$$\frac{\Delta_i}{\Delta_e} = \frac{3\pi A}{2A_c} \sum_{m=0}^{\infty} \sum_{n=0}^{\infty} \frac{\chi_{mn} J_1^2 \left(2\pi a \sqrt{m^2+n^2}/s \right)}{\left(2\pi a \sqrt{m^2+n^2}/s \right)^3} \,. \tag{14}$$

The calculated dependence of Δ_i/Δ_e on the ratio a/s ranging from 0 to 0.5 is shown in Fig. 2, where $a/s = 0$ corresponds to the case when s and l go to the infinity. It is easy to see that for the values of a/s, which are smaller than 0.2, the exact calculation results can be well approximated by the simple linear relation

$$\Delta_i/\Delta_e = 1 - 2.27\, a/s \,. \tag{15}$$

A resonance in the system will occur when the reactance X is equal to zero; then using Eq. (12) the resonance equation can be written as

$$\cot(kl) = A_c k(d+\Delta)/A \,. \tag{16}$$

Frequencies computed from this condition correspond to the natural resonance frequencies of the system. Now, assume that a frequency of excitation was chosen as to tune the system to the lowest resonance mode. It is easy to see that it is equivalent to the condition $kl < \pi/2$ in Eq. (16). When the resonator geometry is such that the non-dimensional

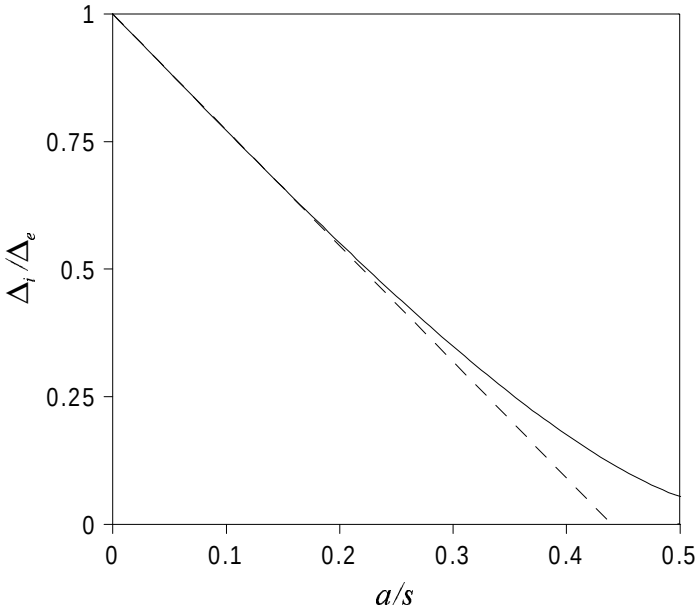

Fig. 2. Ratio of the internal end correction Δ_i to the external end correction Δ_e versus a/s for the resonator cavity with a square cross-section. Solid line – Eq. (14), dashed line – Eq. (15).

parameter kl at resonance is much smaller than unity, the solution of Eq. (16) gives the classical formula for the frequency of the Helmholtz mode

$$f_0 \simeq \frac{c}{2\pi}\sqrt{\frac{A}{V(d+\Delta)}}\,, \tag{17}$$

where V is the volume of the resonator cavity. The range of values of kl can be extended if one uses the approximation: $\cot(kl) \simeq 1/kl - kl/3$. In this case Eq. (16) yields

$$f_0 \simeq \frac{c}{2\pi}\sqrt{\frac{A}{V(d+\Delta)+(1/3)Al^2}}\,. \tag{18}$$

As may be seen, the term preceded by $1/3$ is the difference between the classical formula and Eq. (18) only. When kl is close to $\pi/2$ the expression $\cot(kl) \simeq \pi/2 - kl$ is a better approximation of the cotangent function and its use gives

$$f_0 \simeq \frac{c}{4\left[l + A_c(d+\Delta)/A\right]}\,, \tag{19}$$

which is the well-known formula for the frequency of one quarter-wave resonance.

The sharpness of resonance is characterized by the quality factor Q of the system which for the Helmholtz mode is defined by [13]

$$Q = \frac{\omega_0 M}{R_0} = \frac{\rho c}{k_0 R_0 V}, \tag{20}$$

where $\omega_0 = 2\pi f_0$, $k_0 = \omega_0/c$, $M = \rho(d+\Delta)/A$ is the total effective mass in the resonator orifice and R_0 is the resistance R determined for the resonance frequency. If one uses Eq. (20) as the definition of the quality factor for higher values of the parameter kl, then comparing Eq. (11) with Eq. (20) it is easy to see that

$$Q = \left|\frac{p(l)}{P}\right|_0 \frac{\sin(k_0 l)}{k_0 l} \,, \tag{21}$$

where the index "0" denotes that the ratio $p(l)/P$ is determined for the resonance frequency. Equation (21) shows that the quality factor can be determined experimentally when the frequency f_0', at which $|p(l)/P|$ peaks, is very close to f_0. The difference between f_0' and f_0 is the result of energy loss in the resonator, therefore f_0' is usually called the damped resonance frequency. The relation between f_0' and f_0 can be simply determined for the Helmholtz mode only. If the radiation resistance R_r is much larger than the viscous loss resistance R_o, then from Eq. (11) one obtains

$$\left|\frac{p(l)}{P}\right| = \frac{1}{\dfrac{f}{f_0}\sqrt{\left(\dfrac{f}{f_0}-\dfrac{f_0}{f}\right)^2 + \dfrac{1}{Q^2}\left(\dfrac{f}{f_0}\right)^4}} \,. \tag{22}$$

From Eq. (22) a formula for the frequency f_0' can be found and the result is

$$f_0' = \frac{f_0}{\sqrt{3}}\sqrt{Q\sqrt{Q^2+6}-Q^2} \,. \tag{23}$$

Now, if the viscous loss resistance is much larger than the radiation resistance, from Eq. (11) the following expression can be derived

$$\left|\frac{p(l)}{P}\right| = \frac{1}{\dfrac{f}{f_0}\sqrt{\left(\dfrac{f}{f_0}-\dfrac{f_0}{f}\right)^2 + \dfrac{1}{Q^2}\dfrac{f}{f_0}}} \,, \tag{24}$$

which leads to the following formula for the frequency f_0'

$$f_0' = \frac{f_0(\sqrt{64Q^4+9}-3)}{8Q^2} \,. \tag{25}$$

Figure 3 shows the dependencies of f_0'/f_0 on Q calculated from Eqs. (23) and (25). From these data it results that the frequencies f_0' and f_0 substantially differ for small values of Q. However, when the quality factor is larger than 10, the difference between f_0' and f_0 becomes negligible. Thus, if the value of Q for the considered resonator is within this range, from the measured frequency dependence of $|p(l)/P|$ it is possible to predict:

- the natural resonance frequency f_0 as the frequency at which $|p(l)/P|$ peaks,
- the quality factor Q as a product of the maximum value of $|p(l)/P|$ and $\sin(k_0 l)/k_0 l$.

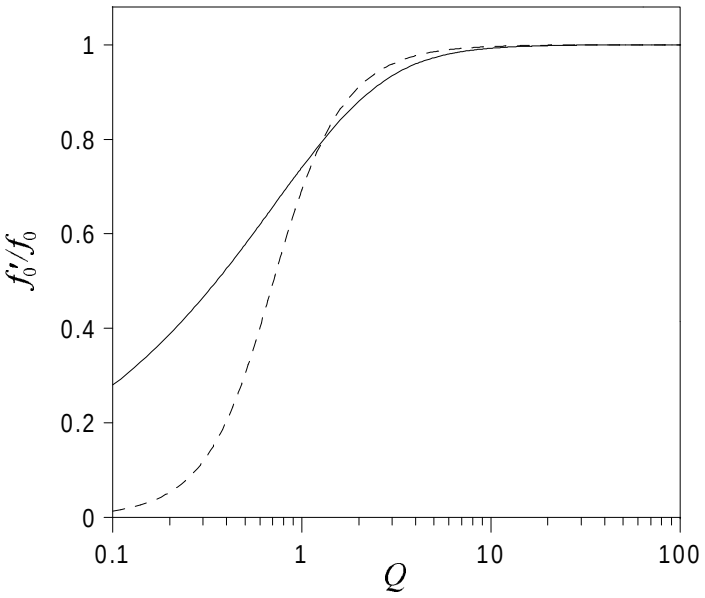

Fig. 3. Dependence of the ratio f_0'/f_0 on the quality factor Q. Solid line – Eq. (23), dashed line – Eq. (25).

3. Experimental investigations

3.1. Procedure and equipment

The resonator used in the tests had the form of a parallelepiped with a square cross-section ($s = w = 5$ cm) and the length l ranging from 1 to 16 cm (Fig. 4). A sharp-edged circular orifice with the radius $a = 6$ mm and the thickness $d = 0.5$ mm was located symmetrically with relation to the lateral cavity walls. The tests were carried out in the laboratory arrangement shown in Fig. 5. The acoustic signal in the form of a plane wave was produced by the broad-band Goodmans loudspeaker having a diameter of 30 cm. The loudspeaker was supplied by Brüel and Kjær (B&K) type 1024 generator. The white noise with a total sound level of 100 dB was applied as the excitation signal.

In the tests a B&K type 2033 narrow-band analyser was used. The analyser has one channel only, but it possesses a number of modes which are very useful in the spectra analysis and some of them, which seem to be the most important, are: the linear spectra averaging, the recording of one spectrum in the internal memory and the function "Input/Memory" which enables the determination of the ratio between the signal on the analyser input and the signal recorded in the memory. The first stage of the tests contained a measurement of the amplitude $|P|$ of the incident pressure signal within the considered frequency range. It was performed for a closed resonator orifice in order to eliminate the signal radiated by the resonator. The incident pressure was measured by a $1/4''$ B&K microphone mounted just before the rigid plate closing the resonator

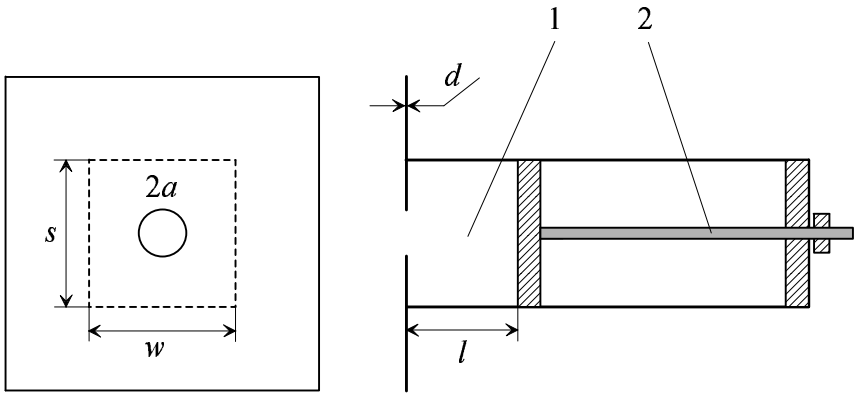

Fig. 4. Sketch of the resonator construction. 1 – resonator cavity, 2 – rod joining the casing of the mechanical system with the piston closing the resonator cavity.

cavity (Fig. 5). To eliminate the errors due to pressure fluctuations, the linear averaging with 1024 samples was used. A spectrum of the incident pressure was recorded in the analyser memory. In the second stage of the tests, the resonator orifice was opened and for the same generator settings the pressure amplitude $|p(l)|$ was measured. It was done by the $1/4''$ B&K microphone mounted at the bottom end of the resonator cavity (Fig. 5). A spectrum of $|p(l)|$ was determined after the linear averaging with 1024 samples also. Finally, the ratio between $|p(l)|$ and $|P|$ was found using the function "Input/Memory" of the analyser.

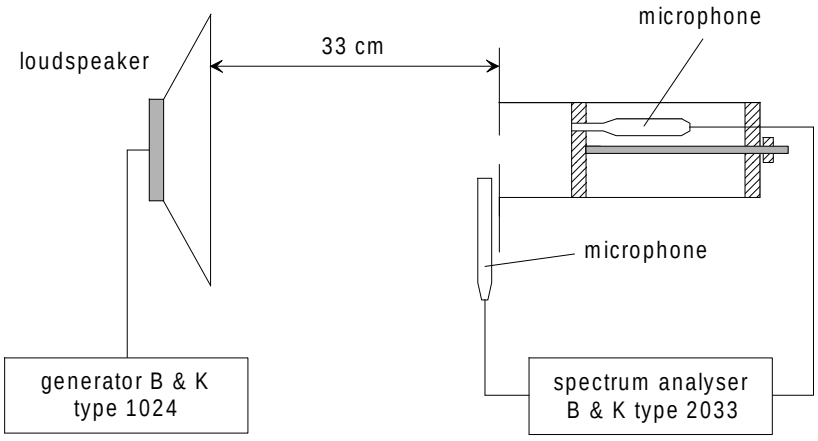

Fig. 5. Setup for the resonator response measurements.

With the analyser 2033 the frequency analysis of the pressure signal can be made within the defined frequency range. The accuracy of the frequency measurement is the same at a given frequency range. In order to locate the maximum in the $|p(l)/P|$ curve,

the preliminary tests were performed within the frequency range up to 2000 Hz where the accuracy of the frequency readout is 5 Hz. The graph in Fig. 6 is an example of the measured frequency response of the resonator. It was obtained for the resonator length l of 10 cm. In this case the resonance frequency f_0 and the quality factor Q of the system as measured from the response curve were 370 Hz and 25, respectively.

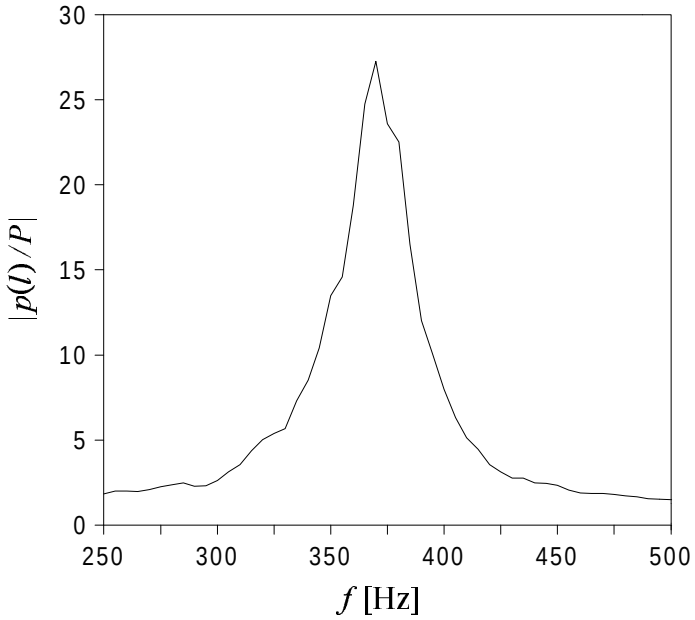

Fig. 6. Frequency dependence of $|p(l)/P|$ for the resonator length $l = 10$ cm.

3.2. Comparison of experimental data to theoretical predictions

In the resonance frequency measurements the "Zoom" function of the analyser 2033 was used giving the frequency readout with the accuracy of 0.5 Hz. In Fig. 7a experimental data compared with the three resonance frequency contours are shown. The graph marked by the solid line was computed numerically from Eq. (16) – the exact resonance equation, however the theoretical data denoted by the dashed line and the dashed-dotted line were obtained from Eq. (17) for the frequency of the Helmholtz mode and Eq. (19) for the frequency of the one-quarter wave resonance. The internal end correction Δ_i, which is necessary for the frequency prediction, was calculated numerically from Eq. (13b) for small resonator lengths ($l \leq 4$), whereas for the remaining values of l, the approximate formula (15) was used. The results calculated from Eq. (18) are not presented in Fig. 7a because for the considered resonator lengths they agree almost exactly with the results obtained from Eq. (16). The disagreement between Eq. (16) and the approximate formula is less than 0.6% and corresponds to the frequency difference smaller than 1.5 Hz.

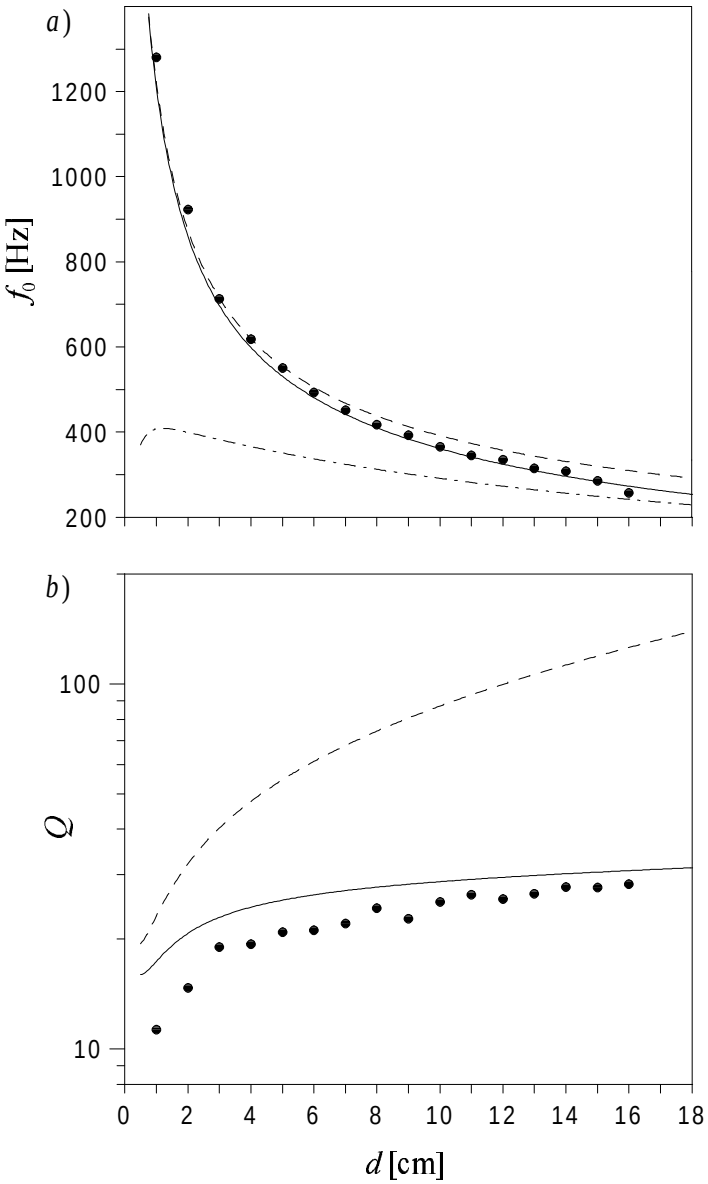

Fig. 7. Comparison of experimental data to theoretical predictions, (a) resonance frequency: solid line – Eq. (16), dashed line – Eq. (17), dashed-dotted line – Eq. (19), points – experiment, (b) quality factor: solid line – Eq. (20), dashed line – Eq. (20) without viscous loss resistance, points – experiment.

As shown in Fig. 7a, the theory predicts reasonably well the resonance frequency f_0 of the system. The discrepancy between the experimental data and the results obtained from Eq. (16) is less than 6.8% for all resonator lengths, and the agreement is improving as the resonator length l is increased. The precision of Eq. (17) in predicting the

resonance frequency is sufficient for $l \leq 6$ cm, however for larger values of l a higher deviation from the experimental data, connected with the approximation of the cotangent function by only the first term of the series expansion, is clearly seen. In contrast to Eq. (17), the accuracy of the formula (19) increases with growing resonator length and is satisfactory for the largest values of l.

In Fig. 7b a comparison of the quality factor experimental data to theoretical predictions is presented. Calculation results denoted by the solid line were obtained from Eq. (20), in which all resistive components were included. These results follow the experimental data, but are slightly higher, suggesting that the theory predicts somewhat lower losses in the resonator under consideration. The curve marked by the dashed line depicts computational results obtained in the case when the viscous dissipation in the resonator orifice is neglected and acoustic energy losses in the system are due to a radiation only. From a comparison of the theoretical curves it follows that radiation losses are dominant in a range of very small resonator lengths and they result from the fact that the radiation resistance is proportional to a square of the wave number.

3.3. Influence of mechanical vibrations on the resonator response

It was found that for some resonator lengths the acoustic response of the system was considerably deformed because of sudden drops in the cavity pressure near two frequencies. The first pressure drop was observed for the resonator length ranging from 0.8 to 1.1 cm and it appeared at the frequency close to 1320 Hz. The second pressure drop, which occurred near the frequency of 750 Hz, was detected for $l = 2 - 3$ cm. Figure 8 depicts experimental and theoretical response curves obtained for some values of l from this range. From this figure it results that the frequency f_d, at which a maximal pressure drop was noted, increases little by little with growing the resonator length and the acoustic response of the resonator is much deformed when the frequency f_d is very close to the resonance frequency of the system (Fig. 8b).

In order to locate the source of the acoustic response deformation, the behavior of a mechanical system of resonator under a force excitation was investigated. The mechanical vibration was induced by a impulse force source and its construction was based on the mechanical pendulum scheme. The moving element was a steel frame with a sharp ended rod falling on one of the lateral walls of the resonator. The induced acoustic pulse was measured by the $1/4''$ B&K microphone mounted at the bottom end of the resonator cavity. The tests were performed for the resonator length l from the range $0.8-3.5$ cm. They have shown that in the frequency band $500-1500$ Hz there are two resonance frequencies f_{r1} and f_{r2} of the resonator mechanical system.

The data collected in Table 1 show that f_{r1} and f_{r2} are close to the frequencies f_d at which a pressure drop was observed, thus the deformation of the acoustic response was caused by vibrations of the resonator mechanical system. Moreover, a comparison of f_d to the frequencies f_2 and f_3 indicates that these vibrations are due to the excitation of the second and third eigenmodes of the brass rod joining the casing of the mechanical system with the piston closing the resonator cavity (see Fig. 4). Thus, the response

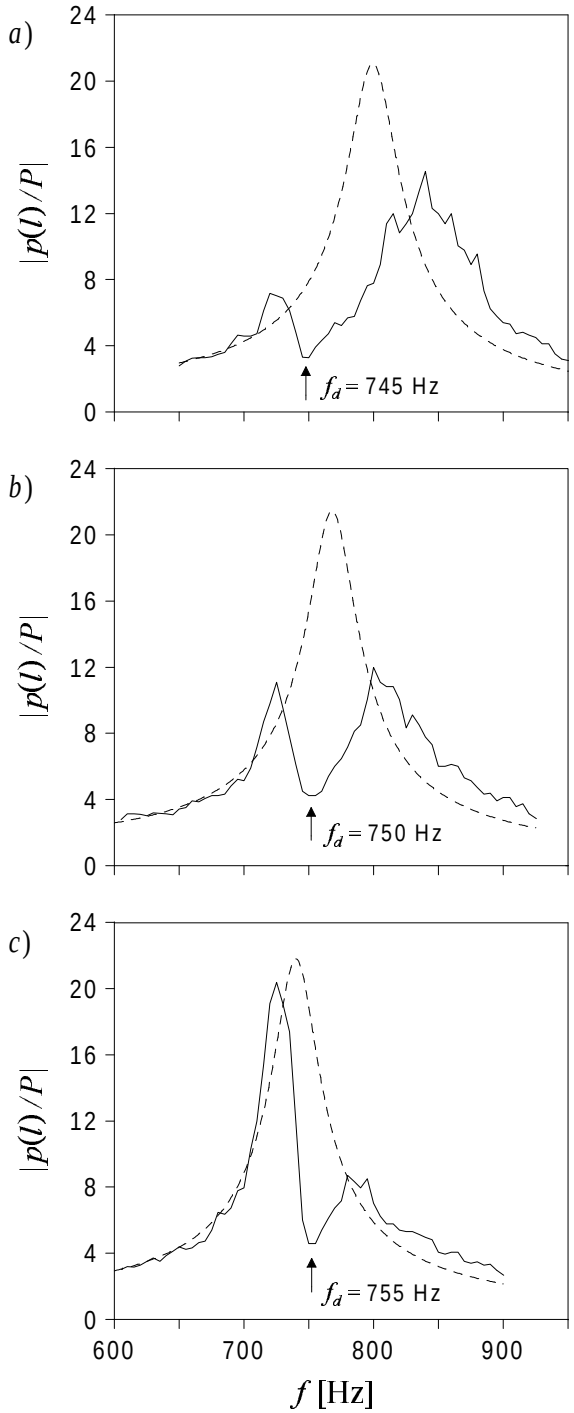

Fig. 8. Deformation of the response curve for the resonator lengths: (a) 2.4 cm, (b) 2.6 cm (c) 2.8 cm. Solid lines – experimental data, dashed lines – calculation results obtained from Eq. (11).

Table 1. Frequencies f_d, f_{r1} and f_{r2} compared with frequencies f_2 and f_3 calculated from Eq. (26).

l [cm]	f_d [Hz]	f_{r1}, f_{r2} [Hz]	f_2, f_3 [Hz]
1	1325	695, 1315	666, 1305
1.5	715	705, 1335	689, 1352
2	735	725, 1365	714, 1400
2.5	750	745, 1390	740, 1452
3	755	750, 1415	768, 1506
3.5	765	770, 1445	797, 1563

deformation results from a suppression of the acoustically excited pressure signal by a mechanically induced acoustic wave. The frequencies f_2 and f_3 were computed from the formula for the rod rigidly supported at both ends [14]

$$f_1 = \frac{0.89D}{L^2}\sqrt{\frac{E_m}{\rho_m}}, \quad f_2 = 2.76f_1, \quad f_3 = 5.4f_1, \tag{26}$$

where ρ_m is the brass density, E_m is the Young's modulus for brass, $D = 5$ mm is the rod diameter and $L = L_{\max} - l$ is the rod length, where $L_{\max} = 30$ cm.

4. Conclusions

The response of the Helmholtz resonator to external excitation by a plane acoustic wave has been investigated in this paper. The theoretical analysis has been presented in order to describe the resonator response as a relation between the pressure induced inside the resonator cavity and the incident pressure. The model of the resonator was based on a lumped-elements approach valid for low frequencies of the excitation.

The theory has shown that for the resonator with a very shallow cavity the internal end correction Δ_i strongly depends on the resonator length [Eq. (13b)]. Moreover, it was found that for a small diameter of the resonator orifice and a cavity with a square cross-section it is possible to calculate Δ_i correctly by using a simple approximate formula [Eq. (15)].

The theoretical analysis has proved that for a lightly damped resonator ($Q > 10$), the natural resonance frequency f_0 of the system and the quality factor Q may be determined directly from the response curve showing the frequency dependence of the ratio of the pressure amplitude at a bottom end of the cavity to the amplitude of the incident pressure. This property was exploited in experimental investigations including measurements of f_0 and Q with a varying resonator length.

A comparison of experimental data to theoretical predictions has shown that for the considered resonator lengths Eq. (18), obtained by retaining the two first terms in the expansion of the cotangent function, approximates very well the frequency calculated

numerically from the exact resonance equation [Eq. (16)], whereas the formulae (17) and (19) have limitations of their range of validity for large and small resonator lengths, respectively. The quality factor predictions are found to be in satisfactory agreement with the experiment.

Finally, the cause of an unexpected deformation of the response curve was investigated. It was found that this deformation was a result of the excitation of the second and third eigenmodes of the brass rod joining the casing of the mechanical system with the piston closing the resonator cavity. These mechanical vibrations produced an acoustic signal in such a phase that a suppression of the pressure inside the resonator cavity occurred.

References

[1] A. ADOBES, I. AUDONNET and E. LUZZATO, *Helmholtz resonators: a numerical package to optimize their design and control their implementation in engineering problems*, Journal of Low Frequency Noise and Vibration, **9**, 92–97 (1990).

[2] R.A. PRYDZ, L.S. WIRT and H.L. KUNTZ, *Transmission loss of a multilayer panel with internal tuned Helmholtz resonators*, J. Acoust. Soc. Amer., **87**, 1597–1602 (1990).

[3] K. NAGAYA, Y. HANO and A. SUDA, *Silencer consisting of two-stage Helmholtz resonator with auto-tuning control*, J. Acoust. Soc. Amer., **110**, 289–295 (2001).

[4] P.A. MONKEWITZ and N. NGUYEN–VO, *The response of Helmholtz resonators to external excitation. Part 1. Single resonators*, J. Fluid Mech., **151**, 477–497 (1985).

[5] R.C. CHANAUD, *Effects of geometry on the resonance frequency of Helmholtz resonators*, J. Sound Vib., **178**, 337-348 (1994).

[6] A. SELAMET, N.S. DICKEY and J.M. NOVAK, *Theoretical, computational and experimental investigation of Helmholtz resonators with fixed volume: lumped versus distributed analysis*, J. Sound Vib., **187**, 358–367 (1995).

[7] N.S. DICKEY and A. SELAMENT, *Helmholtz resonators: one-dimensional limit for small cavity length-to-diameter ratios*, J. Sound Vib., **195**, 512–517 (1996).

[8] A. SELAMET and Z.L. JI, *Circular asymmetric Helmholtz resonators*, J. Acoust. Soc. Amer., **107**, 2360–2369 (2000).

[9] M. MEISSNER, *Absorption properties of Helmholtz resonator at high amplitude incident sound*, Acustica/Acta Acustica, **86**, 985–991 (2000).

[10] U. INGARD, *On the theory and design of acoustic resonators*, J. Acoust. Soc. Amer., **25**, 1037–1061 (1953).

[11] P.M. MORSE and K.U. INGARD, *Theoretical acoustics*, Mc Graw-Hill, New York 1968.

[12] P.M. MORSE and H. FESHBACH, *Methods of theoretical physics*, Mc Graw-Hill, New York 1953.

[13] L.E. KINSLER and A.R. FREY, *Fundamentals of acoustics*, 2nd ed., Wiley, New York 1962.

[14] Z. ŻYSZKOWSKI, *Basics of electoacoustics* [in Polish], WNT, Warsaw 1965.